nature portfolio

https://doi.org/10.1038/s41477-021-00998-8

Supplementary information

Lessons on textile history and fibre durability from a 4,000-year-old Egyptian flax yarn

In the format provided by the authors and unedited

Supplementary information

Preliminary investigations using nanoindentation

Preliminary to the atomic force microscopy measurements, nanoindentation measurements with a Nanoindenteur XP (MTS Nano Instruments, Oak Bridge, Tennessee, USA) used at room temperature and equipped with a three-side pyramid indenter (Berkovich-Berko XPT-12761-0) were used to evaluate the indentation modulus of the samples. Once the indenter touched the surface, the strain rate was set at 0.05 s^{-1} (i.e., 1 µN/s) during loading to reach a depth limit of 120 nm. The load was held at the maximum value for 60 s and then the withdraw was done with the same loading rate up to 10% of the maximum load.

In Supplementary Table 1, nanoindentation moduli (NI) and hardness measured for ancient and modern flax fibres in S_2 layers and embedding resin are reported with their relative standard deviations.

The nanoindentation measurements are in agreement with the AFM PF-QNM analysis and the flax yarn from ancient Egypt seems to have higher indentation modulus than the modern flax yarn.

FTIR-ATR spectroscopy

Material

A small subsample of around 5 mm from both the modern and the ancient flax yarn were directly analysed with a FTIR-ATR spectroscope.

Method

Spectra were acquired at room temperature with a Vertex70v vacuum Fourier Transform Infrared spectrometer (Bruker, USA) equipped with a DLaTGS detector, a KBr window, the KBr beamsplitter and an Attenuated Total Reflection golden gate accessory (germanium cell). Spectra were acquired in absorbance mode with a spectral resolution of 4 cm^{-1} and in a range from 4000 to 600 cm^{-1}.

Both spectra from modern and old yarns were acquired with an accumulation of 64 scans after the background subtraction of a spectrum “in air” with OPUS software (Bruker, USA). The acquisition range was from 500 to 4000 cm^{-1}. The spectra were elastic baseline corrected and unit vector normalized using Opus software (Version 7.5).

XRD investigations

Wide-angle X-ray diffraction (WAXD) measurements were performed under ambient conditions on a Siemens D500 diffractometer CuKα radiation. Scans were collected from 2θ = 5 to 60° with step size of 0.03° at 4 s/step (Fig. 1). The beam was directed perpendicular to the fibre yarn length.

Crystallinity was calculated using Eq. 1, where I_{tot} is the intensity at the primary peak for cellulose I (at 2θ = 22.5°) and I_{am} is the intensity from the amorphous portion evaluated as the minimum intensity (at 2θ = 19.0°) between the primary and the secondary peaks (Fig. 1).

$$C = \frac{I_{tot} - I_{am}}{I_{tot}} \times 100 \qquad \text{(Eq. 1)}$$

NMR analysis

NMR investigations were performed on modern and old yarns according to the protocol described in [1]. Solid state 1H/13C CP/MAS NMR experiments were performed on a Bruker Avance III 400 MHz spectrometer with a ^{13}C frequency of 100.62 MHz by using a double resonance H/X CP/MAS 4 mm probe. The cellulose cell wall crystallinity was calculated by dividing the area of the four peaks of the crystalline region by those of the seven peaks for the cellulose C4 region. The lateral dimensions of the fibrils (LFD) and the lateral dimensions of the fibril aggregates (FLAD) were then estimated using a square model of a cross-section of cellulose microfibril. This work is based on the total cellulosic surfaces of amorphous cellulose and a microfibril model with cellulosic chains 0.57 nm wide[2].

References

1. Bourmaud, A. *et al.* Evolution of flax cell wall ultrastructure and mechanical properties during the retting step. *Carbohydr. Polym.* **206**, 48–56 (2019).
2. Newman, R. H. Estimation of the lateral dimensions of cellulose crystallites using C-13 NMR signal strengths. *Solid State Nucl. Magn. Reson.* **15**, 21–29 (1999).
3. Stewart, D. Fourier Transform Infrared Microspectroscopy of Plant Tissues. *Appl. Spectrosc.* **50**, 357–365 (1996).
4. Garside, P. & Wyeth, P. Identification of Cellulosic Fibres by FTIR Spectroscopy - Thread and Single Fibre Analysis by Attenuated Total Reflectance. *Stud. Conserv.* **48**, 269–275 (2003).
5. Astruc, J. *et al.* Isolation of cellulose-II nanospheres from flax stems and their physical and morphological properties. *Carbohydr. Polym.* **178**, 352–359 (2017).
6. Zhang, H. *et al.* Influence of alkali treatment on flax fiber for use as reinforcements in polylactide stereocomplex composites. *Polym. Eng. Sci.* **55**, 2553–2558 (2015).
7. Lazić, B. D. *et al.* Influence of hemicelluloses and lignin content on structure and sorption properties of flax fibers (Linum usitatissimum L.). *Cellulose* **25**, 697–709 (2018).
8. Margariti, C. The application of FTIR microspectroscopy in a non-invasive and non-destructive way to the study and conservation of mineralised excavated textiles. *Herit. Sci.* **7**, 63 (2019).
9. Mohapatra, H. & Malik, R. Effect of Microorganism on Flax and Linen. *J. Text. Sci. Eng.* **06**, (2015).
10. Kavkler, K., Gunde-Cimerman, N., Zalar, P. & Demšar, A. FTIR spectroscopy of biodegraded historical textiles. *Polym. Degrad. Stab.* **96**, 574–580 (2011).
11. Han, L. *et al.* Even Visually Intact Cell Walls in Waterlogged Archaeological Wood Are Chemically Deteriorated and Mechanically Fragile: A Case of a 170 Year-Old Shipwreck. *Molecules* **25**, 1113 (2020).
12. Titok, V. *et al.* Infrared Spectroscopy of Fiber Flax. *J. Nat. Fibers* **7**, 61–69 (2010).

13. Fan, M., Dai, D. & Huang, B. Transform Infrared Spectroscopy for Natural Fibres. in *Fourier Transform - Materials Analysis* 45–68 (2012).
14. Reynaud, C. *et al.* In-place molecular preservation of cellulose in 5,000-year-old archaeological textiles. *Proc. Natl. Acad. Sci.* **117**, 19670–19676 (2020).
15. Célino, A., Fréour, S., Jacquemin, F. & Casari, P. Characterization and modeling of the moisture diffusion behavior of natural fibers. *J. Appl. Polym. Sci.* **130**, 297–306 (2013).
16. Kavkler, K. & Demsar, A. Application of FTIR and Raman Spectroscopy to Qualitative Analysis of Structural Changes in Cellulosic Fibres. *Tekstilec* **55**, 19–31 (2012).
17. Oh, S. Y. *et al.* Crystalline structure analysis of cellulose treated with sodium hydroxide and carbon dioxide by means of X-ray diffraction and FTIR spectroscopy. *Carbohydr. Res.* **340**, 2376–2391 (2005).
18. Cintrón, M. S. & Hinchliffe, D. J. FT-IR Examination of the Development of Secondary Cell Wall in Cotton Fibers. *Fibers* **3**, 30–40 (2015).
19. Chen, H. L., Jakes, K. A. & Foreman, D. W. SEM, EDS, and FTIR Examination of Archaeological Mineralized Plant Fibers. *Text. Res. J.* **66**, 219–224 (1996).

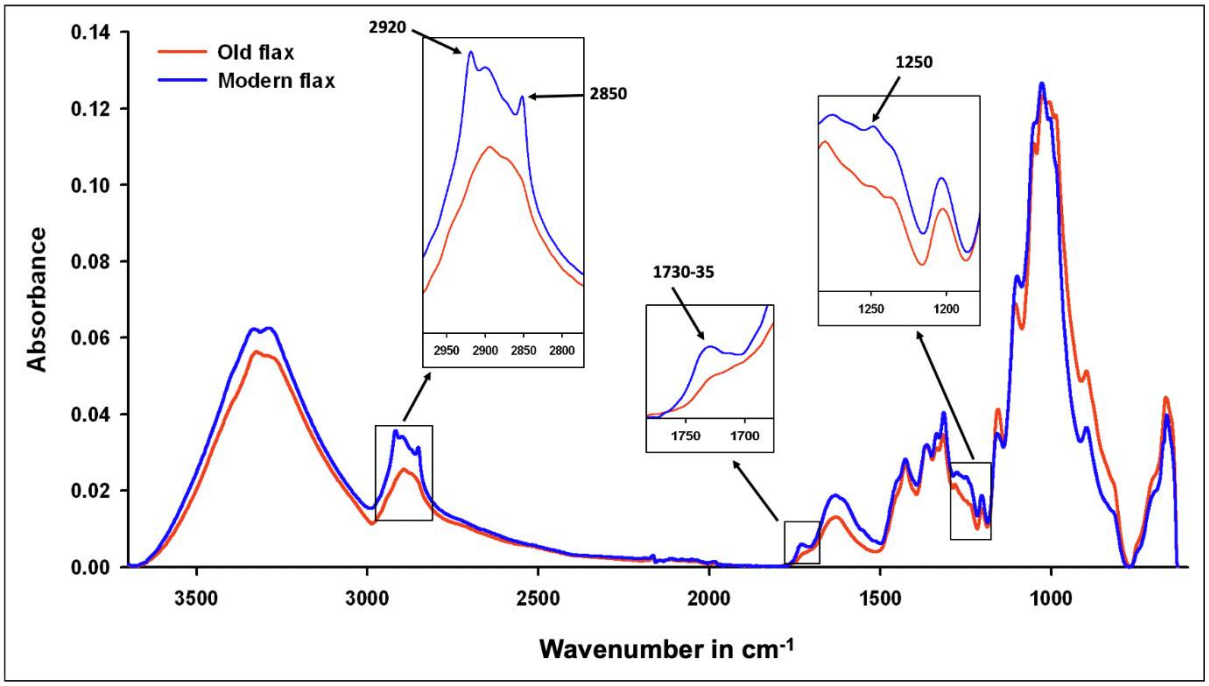

Supplementary Figure 1. FTIR-ATR spectra of modern (blue) and red (Egyptian) flax yarn. baseline subtraction and normalization have been done. Three zones are specifically marked to better highlight differences between the spectra. The main differences between spectra of the modern and ancient flax yarn are in esters carbonyl absorbances (~1730 cm^{-1}) due to the hemicellulose, in the absorbance at ~1247 cm^{-1} of the C-O stretching of the acetyl groups and in the CH stretching of alkyl groups of cellulose and hemicelluloses around 2920 cm^{-1} and 2850 cm^{-1}[3,4]. All these peaks are extremely low in the Egyptian flax yarn compared to the modern one.

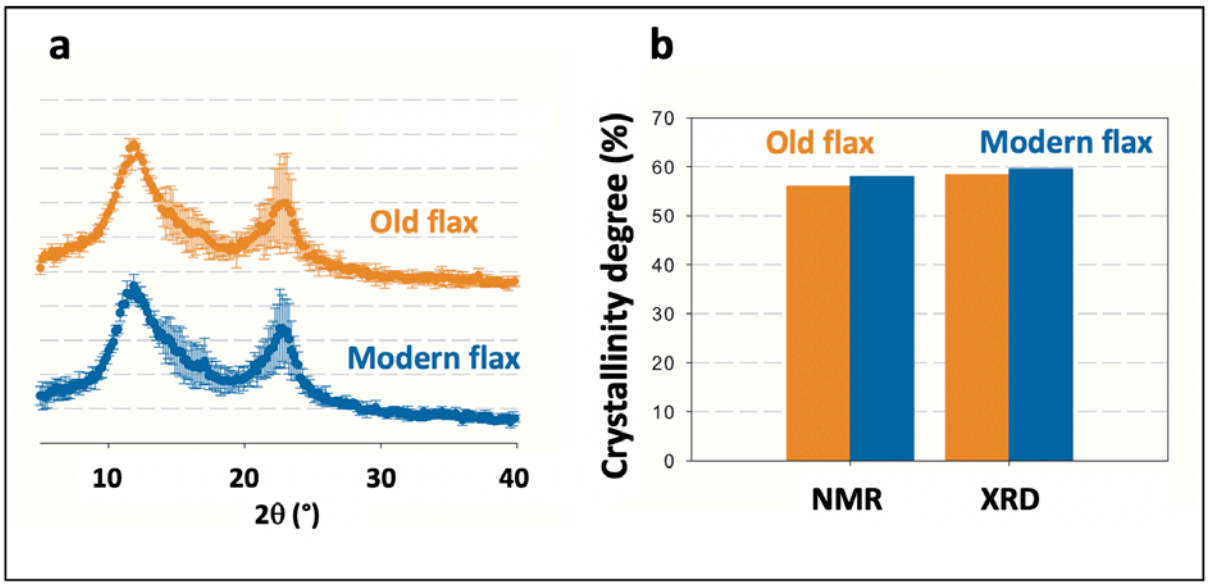

Supplementary Figure 2. XRD spectra of old and modern flax (A) and comparison between crystallinity degree obtained through NMR and XRD investigations (B).

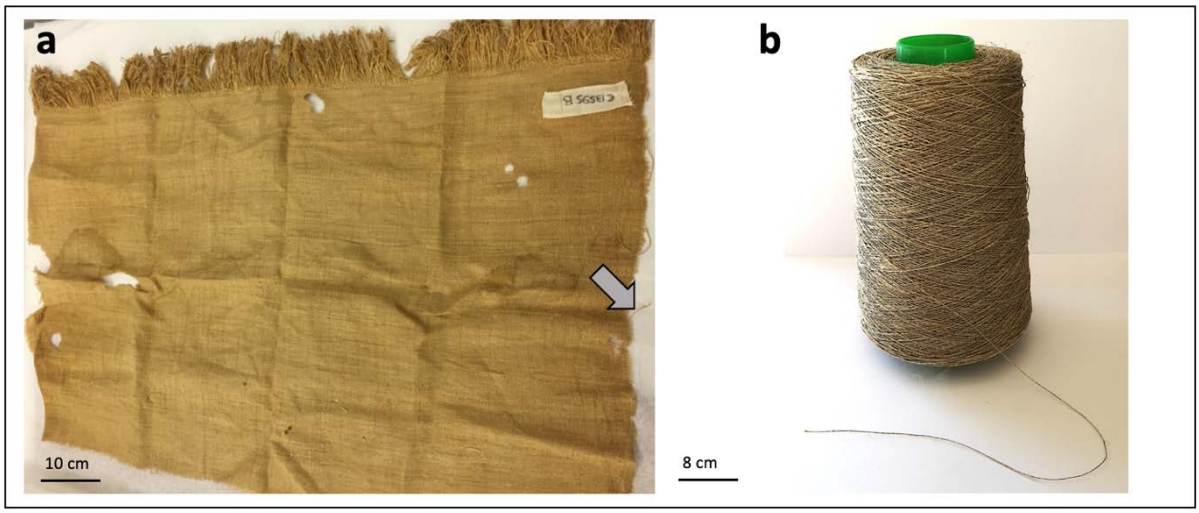

Supplementary Figure 3. Samples used for yarn sampling. Mortuary linen, 2140-1976 BCE (a) and spool of yarn, 2019 AD (b). The yarn collected is indicated by an arrow in the right part of Supplementary Fig.1.a. Images of a object was obtained with the specific permission of Le Louvre Museum.

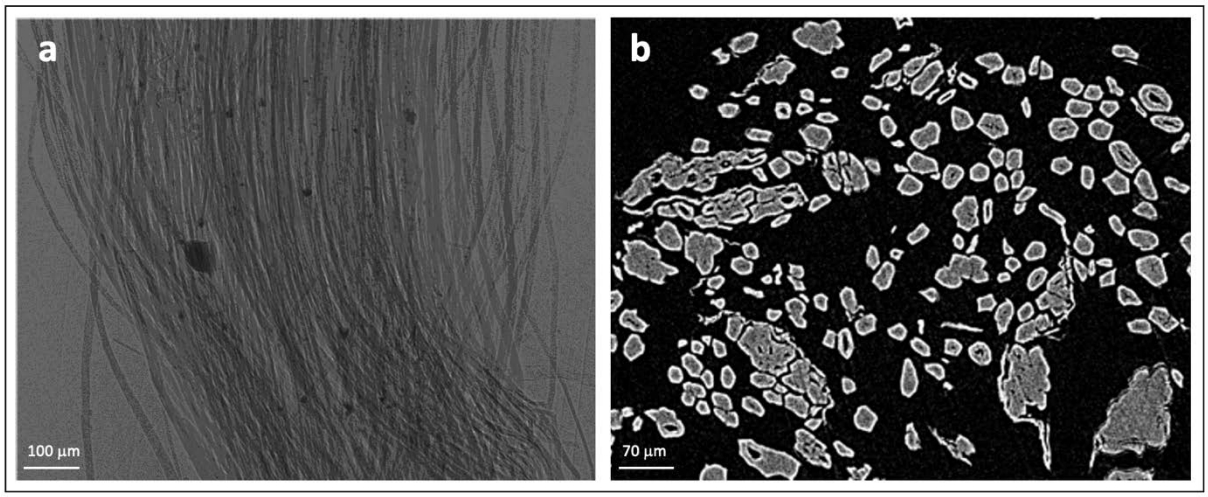

Supplementary Figure 4. Tomographic protocol. Example of X-Ray radiograph on the modern yarn: in Z direction (a) and a slice after reconstruction in Y Direction (b). In (b) one can see

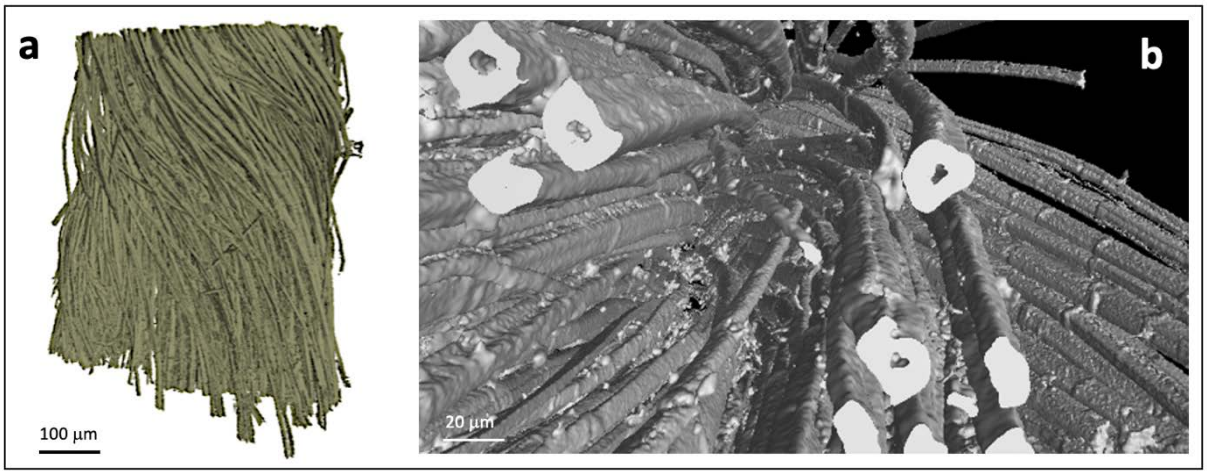

Supplementary Figure 5. Tomographic protocol. Yarn after volume reconstruction at overall (a) and local (b) scale. Nano Tomographic images were acquired from a measured volume of 0.5 mm in diameter over a height of 0.8 mm and each projection obtained was the result of the averaging of 15 acquisitions. Extra images and raw data are available at the following address: https://doi.org/10.17863/CAM.72394.

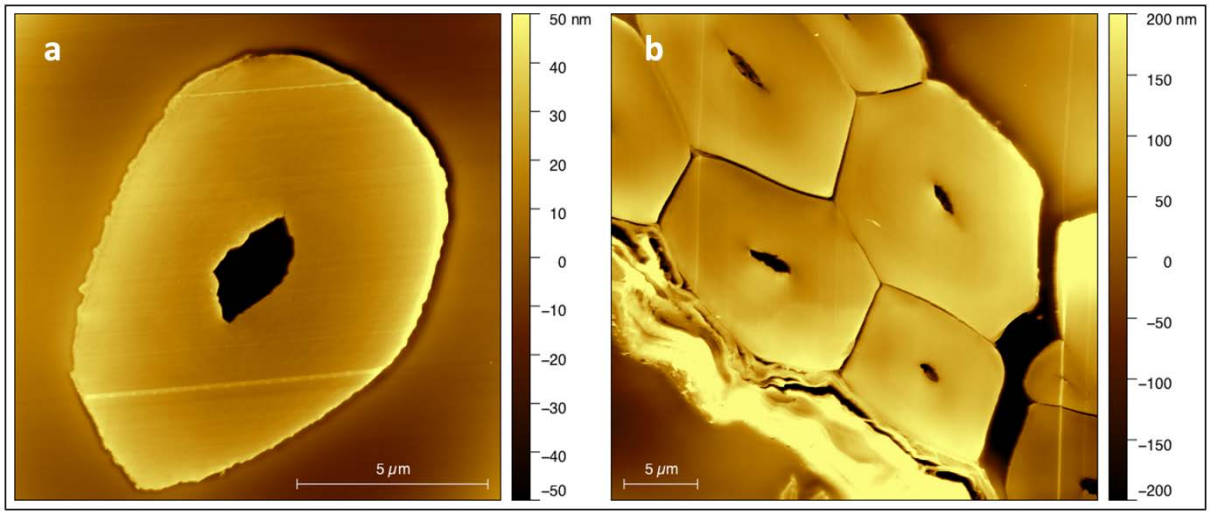

Supplementary Figure 6. Topography images obtained for old (a) and modern (b) yarns by Atomic Force Microscopy (AFM). A good flatness of the images is observed; a more heterogeneous zone appears at the level of the cortical residues for modern flax (b); the structure and the constituents of these regions are different from those of the fibres which can lead to disturbances during cutting. In (a) a single flax fibre can be seen, while in (b) a fibre bundle can be identified. The fibre bundle consists of individual plant cells (fibres) connected by the middle lamella (dark lines). In the lower-left part of the picture, remains of the parenchyma can be found. Two to three different areas of each sample (old and modern respectively) were measured to obtain a better statistic. Extra images and raw data are available at the following address: https://doi.org/10.17863/CAM.72394.

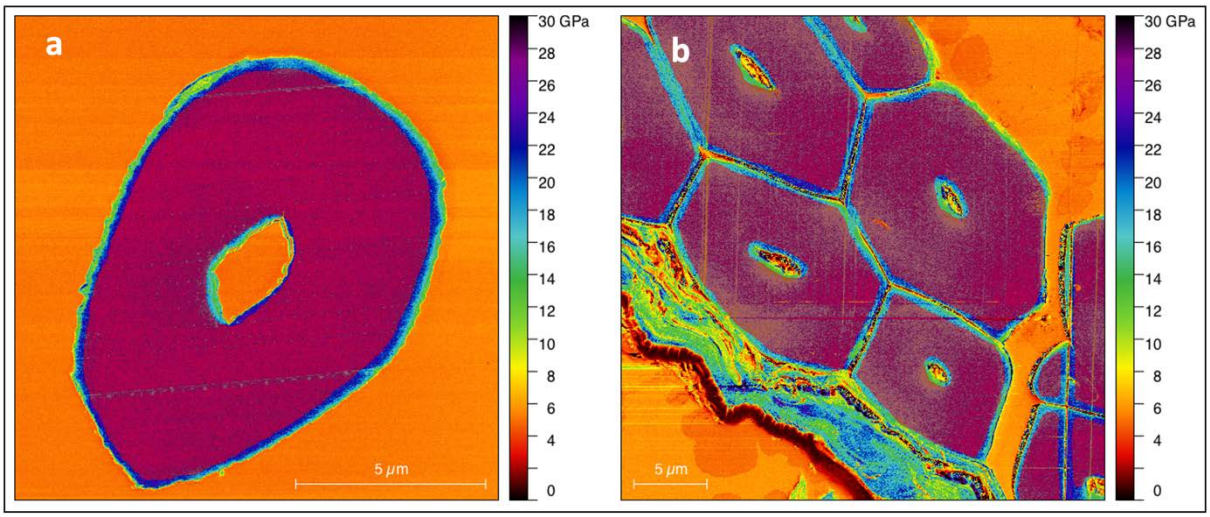

Supplementary Figure 7. Data treatment of AFM-PF-QNM investigations. The purple mask represents the areas used to collect the data for Figure 4.e. Similar calculations were performed on the other images for modern and old yarn. Two to three different areas of each sample (old and modern respectively) were measured to obtain a better statistic. Extra images and raw data are available at the following address: https://doi.org/10.17863/CAM.72394. The indentation modulus calculated were obtained from two or three separate images and from between 80,000 and 140,000 points for each image analysed.

Tables

Sample		Number of tests	Indentation modulus in GPa	Standard Deviation in GPa	Hardness in MPa	Standard Deviation in MPa
Old Sample	Fibre	23	23.9	± 3.48	430	± 70
	Resin	15	5.10	± 0.20	236	± 5
Modern fibre	Fibre	35	20.7	± 2.93	396	± 55
	Resin	23	5.30	± 0.25	250	± 19

Supplementary Table 1. Nanoindentation modulus and hardness obtained on fibre and resin for old and modern flax samples.

Position (cm^{-1}) in Egyptian and modern flax yarn	Position (cm^{-1}) assigned in literature	Assignment (literature)	Reference
~ 3334 to 3286	~ 3600 to 3000	Hydrogen bonded OH (hydroxyl group) stretching vibration in cellulose, hemicellulose and lignin	[4–7]
~ 2920	~ 2920	vC-H stretching vibration in cellulose and hemicellulose	[5,6]
~ 2895	~ 2900	vC-H general organic material content of the fibre, polysaccharides	[4,8]
~ 2850	~ 2850	vC-H_2 in cellulose, hemicellulose and lignin	[9,8,4–6]
~ 1730	~ 1730-1735	Carbonyl C=O and carboxyl stretching of carboxylic acid or ester group of hemicelluloses	[3–7,9–11]
~ 1635	~ 1635	Absorbed water	[4,7–9]
~ 1595 (present in modern but absent in old flax yarn)	~ 1595	vC=C aromatic in plane Lignin	[3,4,8,12]
~ 1515 present in modern but absent in old flax yarn)	~ 1510	vC-C aromatic in plane Lignin	[4,3,12]
~ 1450	~ 1455	δC-H; δC-OH 1° and 2° alcohol	[4,5]
~ 1425	~ 1420	δOCH and δHCH in plane, crystalline cellulose	[4,13–15]
~ 1365	~ 1365-1370	δC-H and δCOH of cellulose, hemicellulose	[14,16]
~ 1334	~ 1335	δCH_2 and δCOH, mainly cellulose	[4,8,14,17]
~ 1315	~ 1315	δCH_2 wagging and δCOH of cellulose, hemicellulose	[15]
~1280	~1280	δCH	[16,17]
~ 1247	~ 1250	vC-O hemicellulose polysaccharides, lignin	[13,14]
~ 1234	~1235	vC-O in lignin and δC-OH in cellulose	[14,17]
~ 1203	~ 1200	δC-OH; δC-CH	[4,14,17]
~ 1157	~ 1155	v_{as}C-O-C; vC-C ring breathing	[~~14,16~~]
~ 1105 for old flax yarn ~1099 for modern flax yarn	~ 1105	vC-O 2° alcohol; vC-O-C glycosidic (mainly cellulose)	[14,18]
~ 1050	~ 1050	vC-OH 2° alcohol	[18]
~ 1025	~ 1025	vC-OH 1° alcohol	[4,8,14,18]
~ 1005	~ 1005	vC-O	[14,18]
~ 985	~ 985	vC-O	[14,17]
~ 895	~ 895	v(C-O-C) in plane in β-Glycosidic bond	[4,8,10,15]

Supplementary Table 2. Correspondence between the peaks recorded in FTIR and the main constituents of the flax cell walls. All of these data come from literature. The shaded lines correspond to the peaks highlighted in Supplementary Fig.6; they underline the main differences related to peaks attributed to hemicelluloses, between spectra of the modern and old flax yarn.